Supplementary Information

Sustainable highly charged C_{60}-functionalized Polyimide in non-contact mode triboelectric nanogenerator

Jae Won Lee,‡[a] Sungwoo Jung,‡[b] Jinhyung Jo,‡[c] Gi Hyeon Han,[d] Dong-Min Lee,[a] Jiyeon Oh,[b] Hee Jae Hwang,[e] Dukhyun Choi,[e] Sang-Woo Kim,[a] Jun Hee Lee,*[c] Changduk Yang,*[b] and Jeong Min Baik*[a]

[a]School of Advanced Materials Science and Engineering, Sungkyunkwan University (SKKU), Suwon 16419, Republic of Korea.
[b]Department of Energy Engineering, School of Energy and Chemical Engineering, Perovtronics Research Center, Low Dimensional Carbon Materials Center, Ulsan National Institute of Science and Technology (UNIST), Ulsan 44919, Republic of Korea.
[c]School of Energy and Chemical Engineering, Ulsan National Institute of Science and Technology (UNIST), Ulsan 44919, Republic of Korea.
[d]School of Materials Science and Engineering, Ulsan National Institute of Science and Technology (UNIST), Ulsan 44919, Republic of Korea.
[e]Department of Mechanical Engineering, Kyung Hee University, Yongin 17104, Republic of Korea.

*Correspondence to: jbaik97@skku.edu (J. M. Baik); yang@unist.ac.kr (C. Yang); junhee@unist.ac.kr (J. H. Lee)

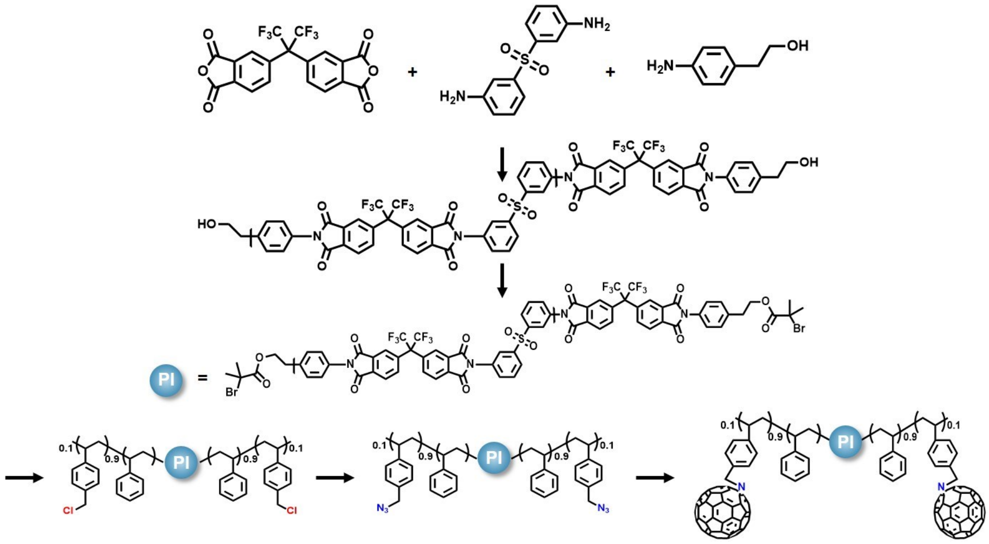

Scheme S1 Scheme for the synthesis of C_{60}–containing polyimides.

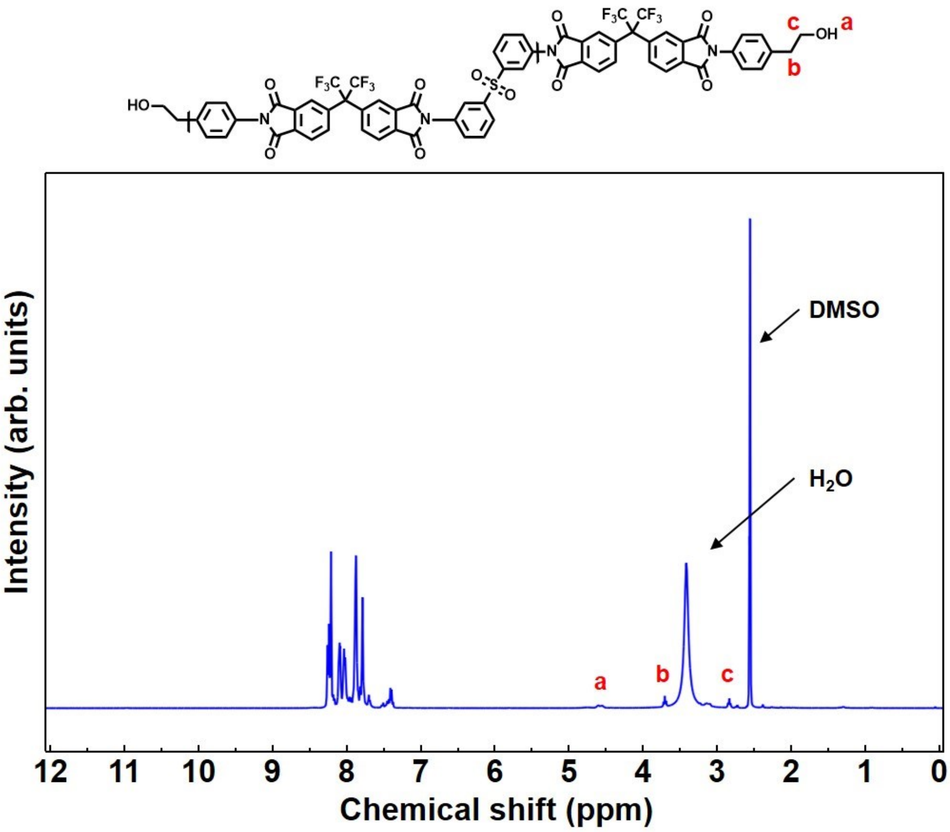

Fig. S1 ^{1}H NMR spectrum of PI with hydroxyl group.

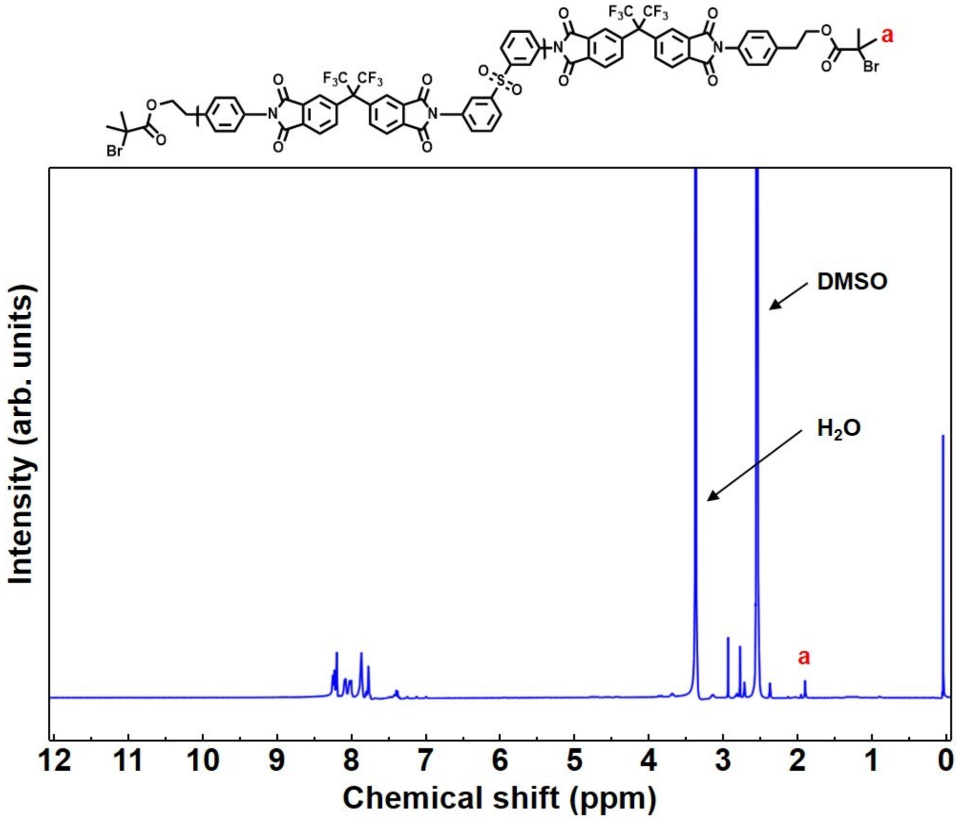

Fig. S2 ^{1}H NMR spectrum of PI macroinitiator.

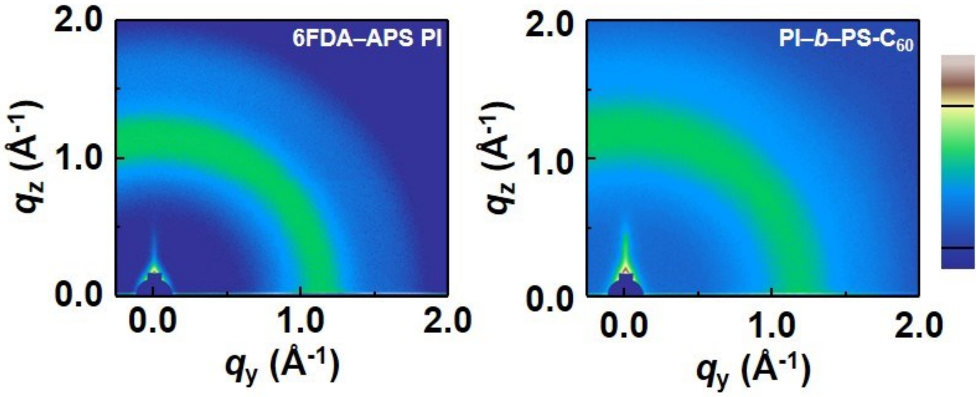

Fig. S3 2D GIWAXS images of the 6FDA–APS PI and PI–*b*–C_{60} films.

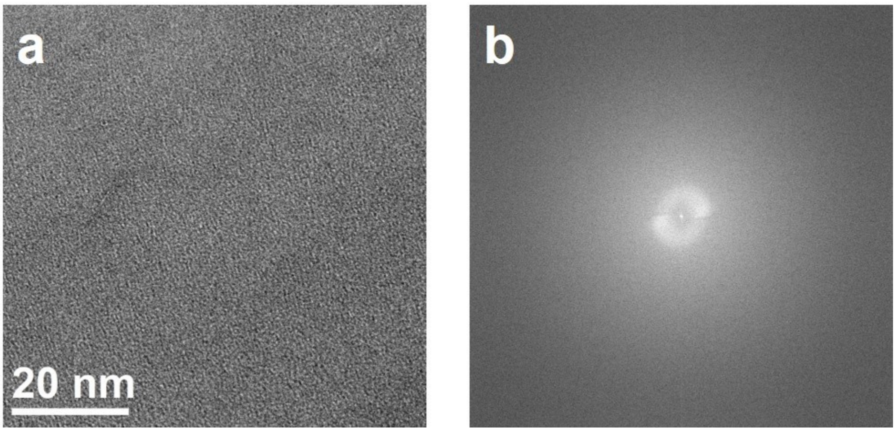

Fig. S4 (a) The TEM image and (b) the selected area diffraction pattern of the PI–*b*–C_{60} films.

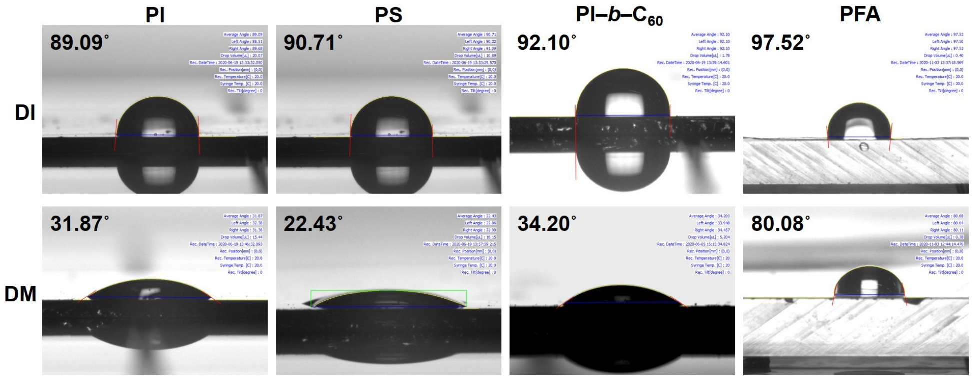

Fig. S5 Side-view goniometer images during static contact angle measurement for the PI, PS, PI–*b*–C_{60}, and PFA films by using DI and DM.

Calculation of surface energy

The surface tensions between donor polymer and SMA were calculated by measuring the contact angles of two different solvents (DI and DM) on each neat film. The surface tension of film was calculated via the Owens-Wendt and the following equations.[1]

$$\gamma_{\mathrm{DI}}(1 + cos\theta_{\mathrm{DI}}) = 4\gamma^{d}_{\mathrm{DI}}r^{d} / (\gamma^{d}_{\mathrm{DI}} + r^{d}) + 4\gamma^{P}_{\mathrm{DI}}r^{P} / (\gamma^{P}_{\mathrm{DI}} + r^{P})$$

$$\gamma_{\mathrm{DI}}(1 + cos\theta_{\mathrm{DM}}) = 4\gamma^{d}_{\mathrm{DI}}r^{d} / (\gamma^{d}_{\mathrm{DM}} + r^{d}) + 4\gamma^{P}_{\mathrm{DM}}r^{P} / (\gamma^{P}_{\mathrm{DM}} + r^{P})$$

$$\gamma^{\ total} = \gamma^{d} + \gamma^{P}$$

where γ^{total} is the total surface tension of material; γ^{d} and γ^{P} are the dispersion and polar components of γ^{total}, respectively. γ_i is the total surface tension of material *i*, where *i* = glycerol or water; γ^{d}_{i} and γ^{p}_{i} a are the dispersion and polar components of γ_i, respectively; θ is the contact angle measured.

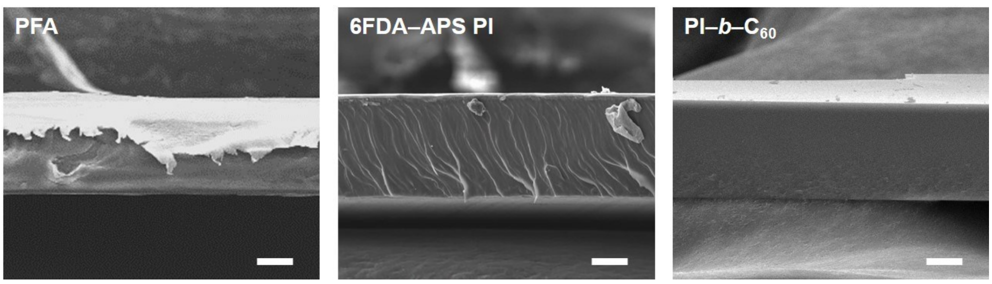

Fig. S6 Cross-sectional SEM images for PFA, 6FDA–APS PI, PI–*b*–C_{60} films. Scale bar, 10 μm.

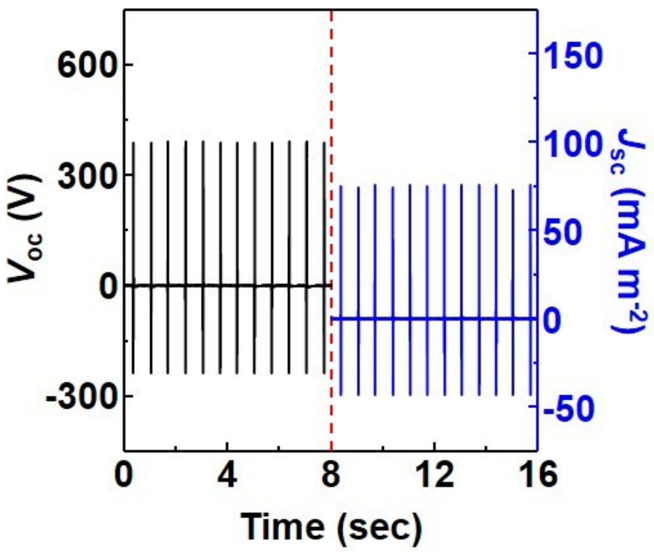

Fig. S7 The V_{oc} and J_{sc} of the TENG with PI–*b*–C_{60} prepared in slow-drying casting at room-temperature.

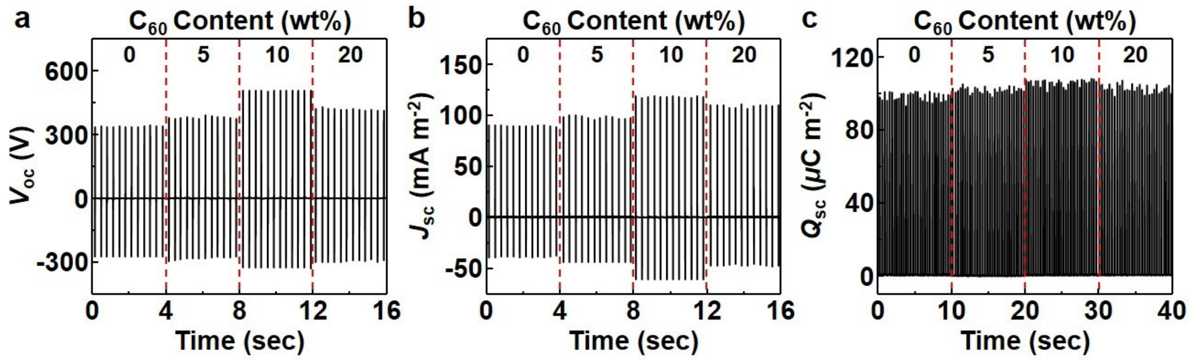

Fig. S8 (a) The output voltages, (b) current densities, and (c) charge densities generated by the PI–*b*–C_{60}-based TENGs as a function of the content of C_{60} ranging from 0 to 20 wt%.

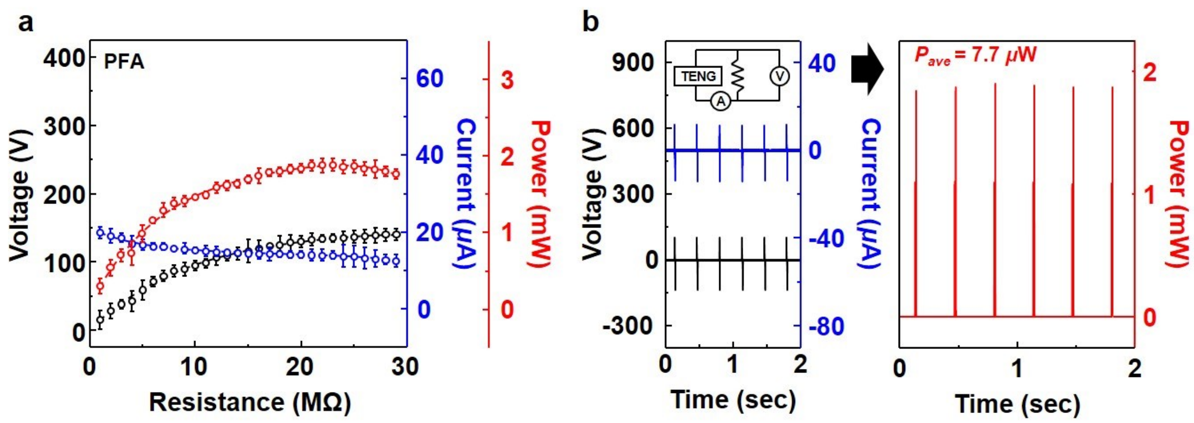

Fig. S9 (a) The instantaneous power of the PFA-based TENG with external loads ranging from 1 to 29 MΩ. (b) Instantaneous output voltage, current, and power of TENG were measured under 23 MΩ. About 7.7 μW of energy was generated under a frequency of 3 Hz.

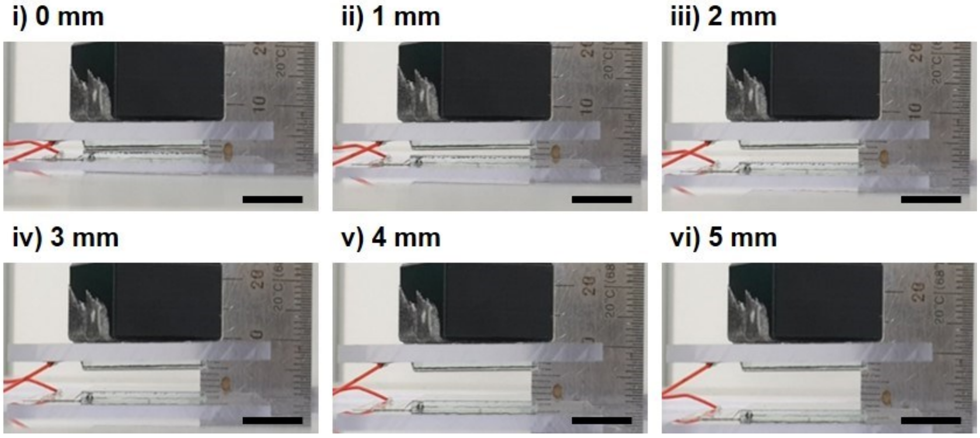

Fig. S10 Images of initial gap for the triboelectric nanogenerator before external forces were applied. Scale bar, 1 cm.

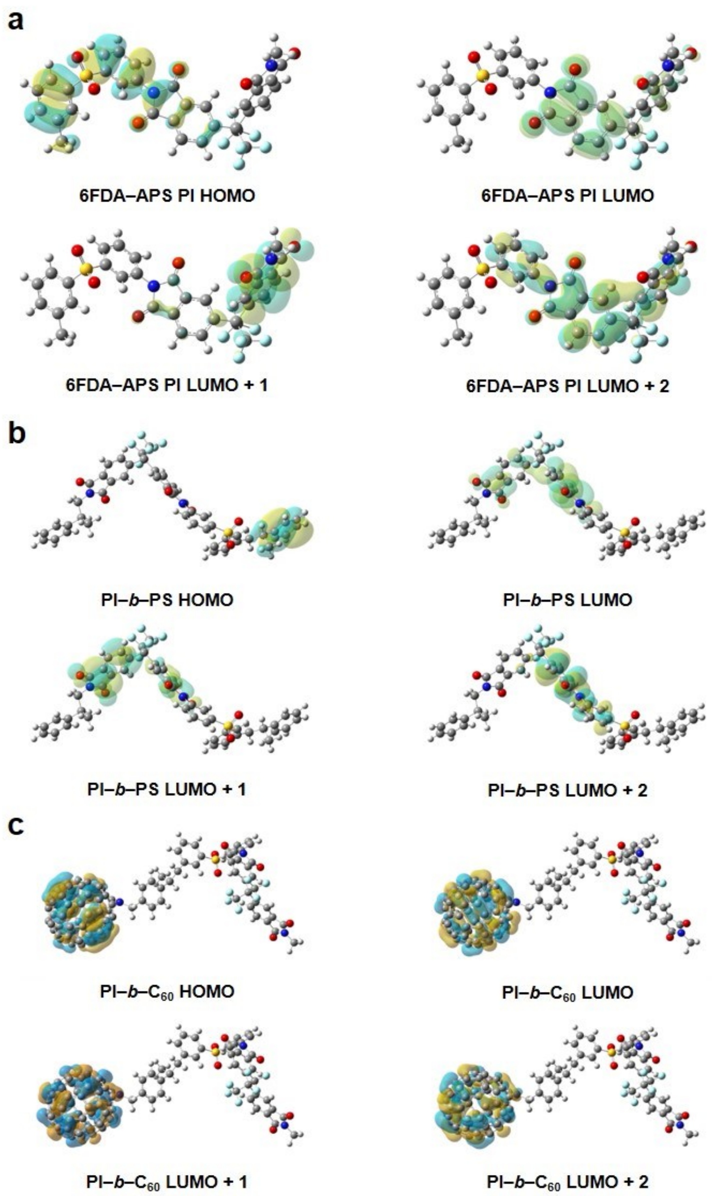

Fig. S11 The molecular orbitals including HOMO, LUMO, LUMO + 1, and LUMO + 2 obtained by DFT calculations with different polymers: (a) 6FDA–APS PI, (b) PI–*b*–PS, (c) PI–*b*–C_{60}. While the molecular orbitals of 6FDS–APS PI and PI–*b*–PS spread out over a particular region of PI backbone, only PI–*b*–C_{60} has the unoccupied molecular orbitals strongly localized to C_{60}. A Gaussian View program was used to visualize the results of molecular orbitals with the iso-surface set to 1×10^{-3} e Å^3. Blue and yellow colors denote the phase difference of the wave function of the orbitals.

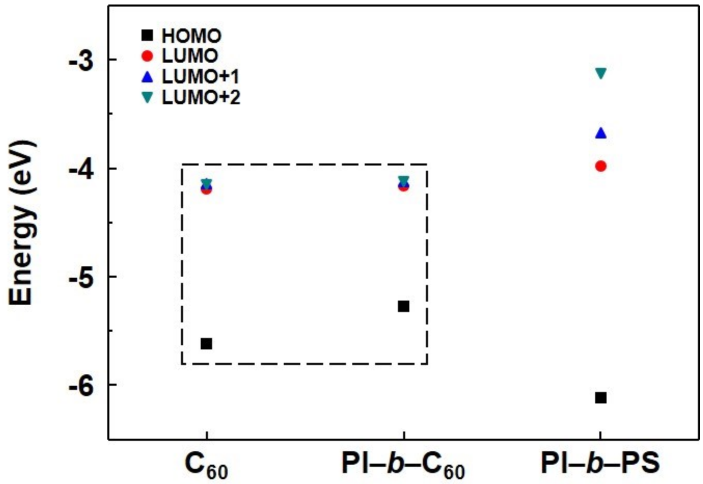

Fig. S12 The molecular orbital energies of C_{60}, PI–*b*–C_{60}, and PI–*b*–PS.

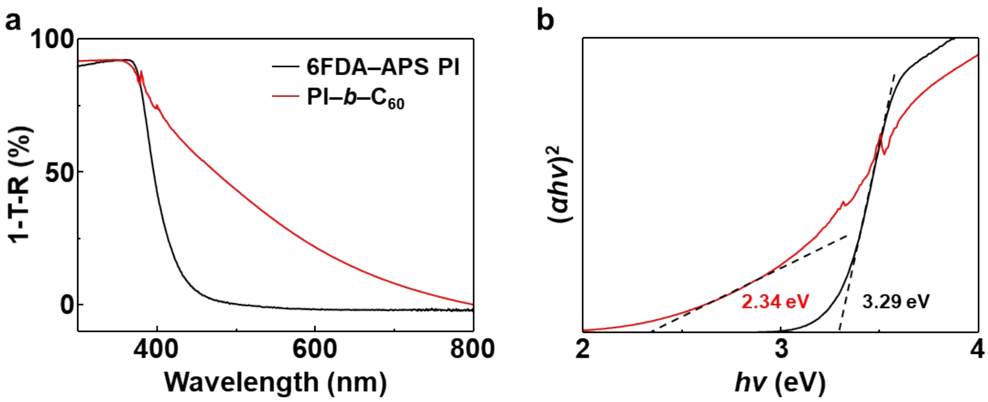

Fig. S13 (a) UV-Vis absorption spectra in the range from 300 to 800 nm. (b) Corresponding plot of transformed Kubelka–Munk function versus the energy of the light.

The E_g^{opt} is calculated by transforming the absorbance by the following equation for the near-edge absorption known as the Kubelka-Munk method, plotted in Fig. S13b.[2]

$$(\alpha h\nu)^2 = h\nu - E_g^{opt} \tag{1}$$

where α is the absorption coefficient and $h\nu$ is the photon energy. The E_g^{opt} of PI–*b*–C_{60} (~2.34 eV) is smaller than that of 6FDA–APS PI (~3.29 eV), which is determined from the intercept of the tangents to the plots of $(\alpha h\nu)^2$ vs the photon energy.

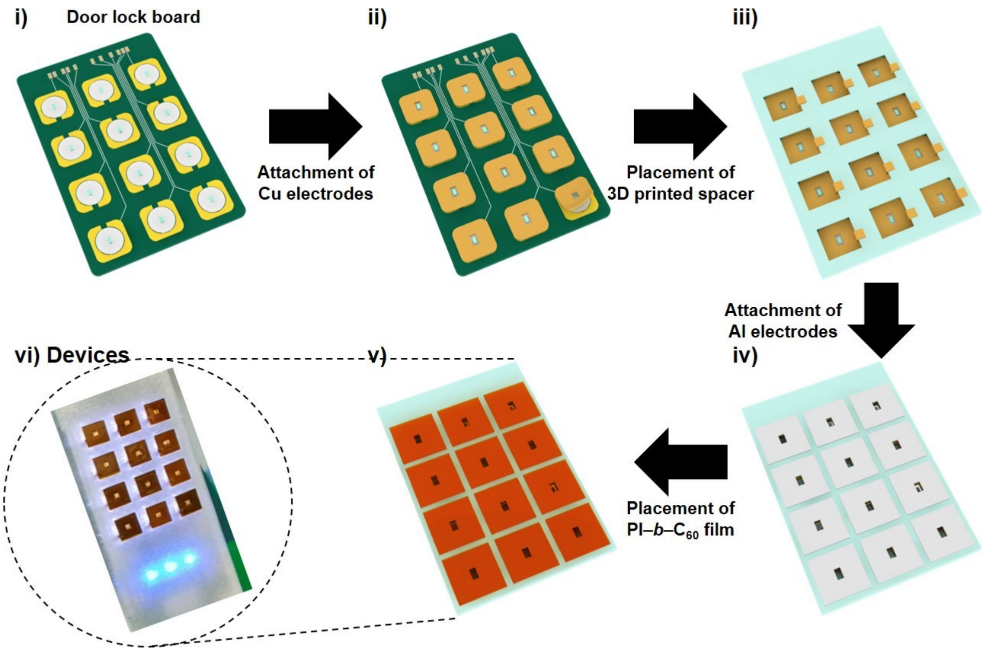

Fig. S14 The schematic diagrams of the fabrication process of a keyless electronic door lock system (i ~ v) and image of the door lock system (vi).

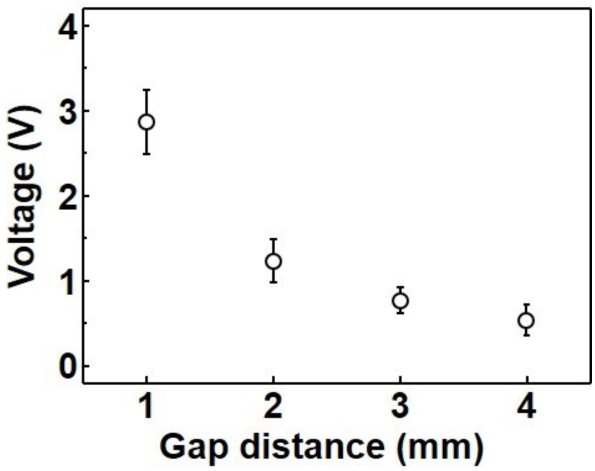

Fig. S15 The average output voltages of the door lock unit when operated by a human finger with a certain distance (1, 2, 3, and 4 mm). Error bars represent standard error of the mean (S.E.M.).

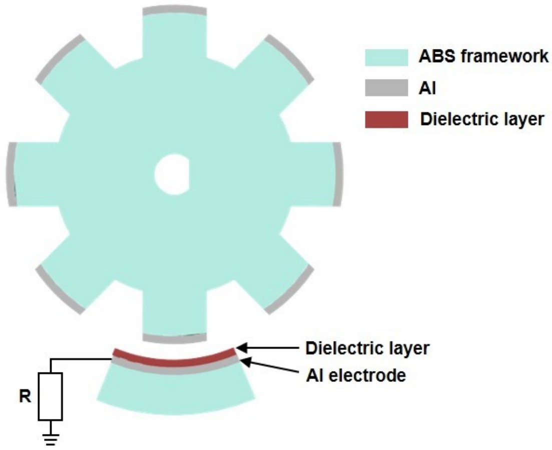

Fig. S16 Schematic of the circuit including the reluctor ring.

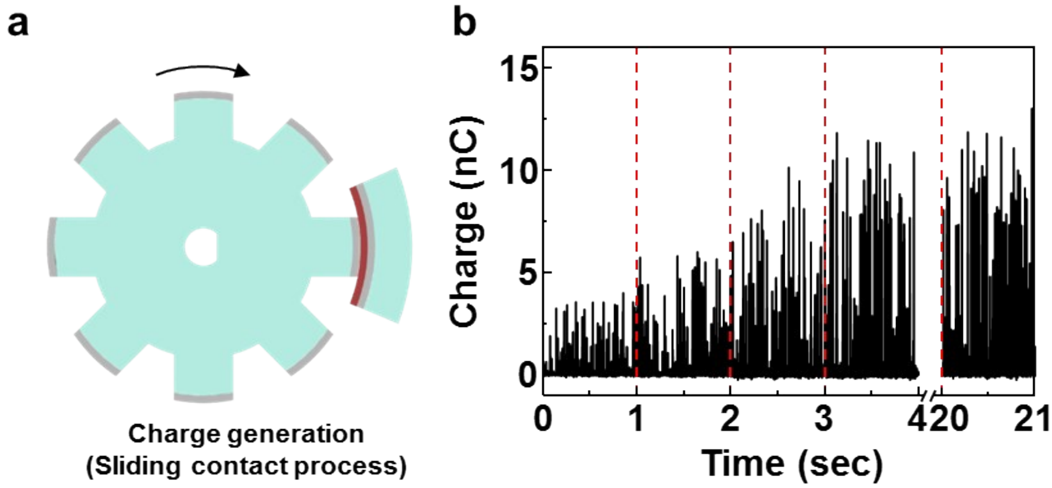

Fig. S17 (a) Schematic illustration of the sliding contact process for charge generation of PI–*b*–C_{60} surface. (b) The charge generated by the sliding contact as a function of contact time.

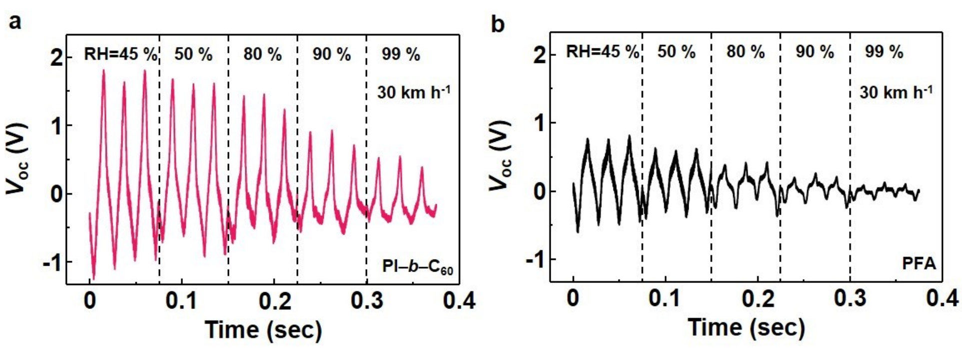

Fig. S18 The V_{oc} generated by speed sensor as a function of relative humidity with different polymers: (a) PI–*b*–C_{60} and (b) PFA.

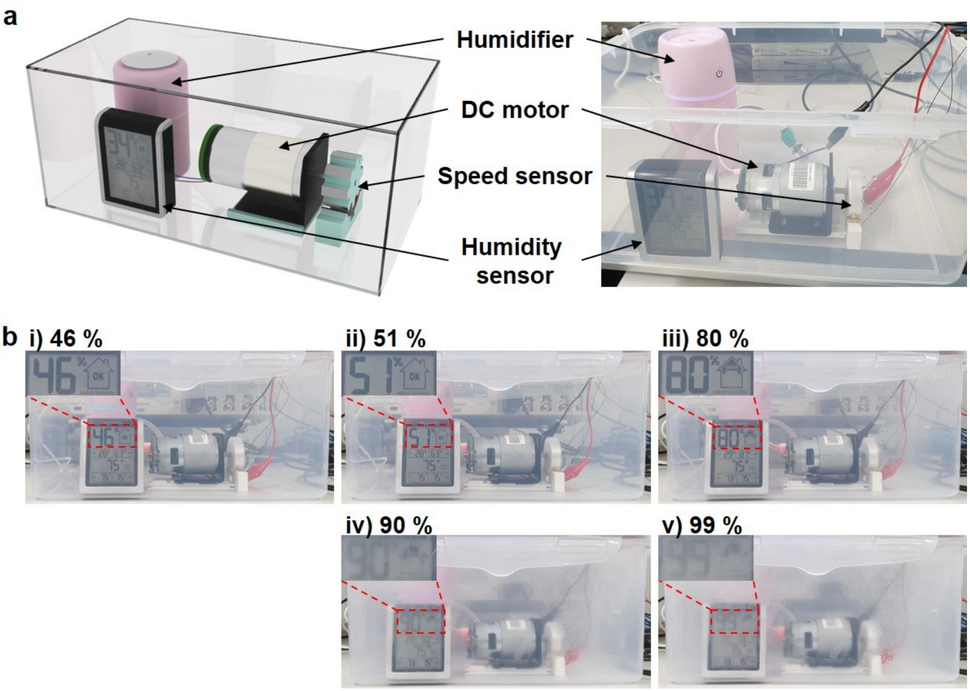

Fig. S19 (a) Schematic illustration and photographs of the humidity system composed of speed sensor with DC motor, humidifier, and humidity sensor. (b) Photographs of the RH value from 45 % to 99 % using humidity sensor.

Table S1 Contact angles and calculated surface energy of PI, PS, PI–*b*–C_{60}, and PFA.

Sample	ϑ_{water} [deg]	ϑ_{DM} [deg]	Surface energy [mN m^{-1}]
PI	89.09	31.87	44.29
PS	90.71	22.43	47.42
PI–*b*–C_{60}	92.10	34.20	43.15
PFA	97.52	80.08	25.73

Table S2 State-of-the-art TENG for power density published recently in top journals.

Schematic Device Structure	Friction material	Power density (mW cm^{-2})	V_{oc} (V)	I_{sc} (μA)	Size / Frequency	Refs.
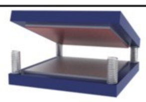	PVDF-PtBA Al	0.45	64.4	75.6	2 × 2 cm^2 / 10 Hz	3
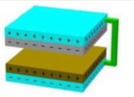	PTFE Tea powder	0.48	792	42.8	5 × 5 cm^2 / 5 Hz	4
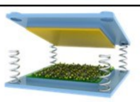	6FDA–APS PI Au NPs/Ag NWs/PDMS	0.71	281.6	30.1	2 × 2 cm^2 / 3 Hz	5
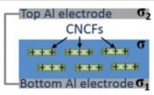	PDMS/CNCFs Al	0.76	320	11.3	1.5 × 1.5 cm^2 / 10 Hz	6
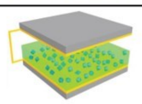	PDMS/HKUST-1 Cu	0.79	205	37	2 × 2 cm^2 / 3.5 Hz	7
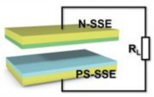	Silicone rubber Nylon	1.12	1170	138	5 × 6 cm^2 / 3 Hz	8
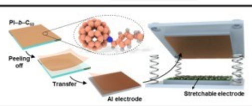	**PI–*b*–C_{60}** **Au NPs/Ag NWs/PDMS**	**1.95**	**337.2**	**35.8**	**2 × 2 cm^2 / 3 Hz**	**This work**

Table S3 Fitting parameters for the exponential decay function in contact mode (d = 0 mm) and non-contact (d = 1 mm) mode from the TENGs fabricated with PFA, 6FDA–APS PI and PI–b–C_{60} films.

Dielectric layer	Distance	τ	ΔQ_D	ζ_L
PFA	d = 0	2.08	0.59	
	d = 1	2.16	0.61	61 %
6FDA–APS PI	d = 0	2.53	0.37	
	d = 1	2.59	0.39	39 %
PI–b–C_{60}	d = 0	2.63	0.17	
	d = 1	2.89	0.19	19 %

Table S4 State-of-the-art TENG for charge retention characteristics published recently in top journals.

Schematic diagram	Material	Surface potential/Output	Surface potential change	Ref.
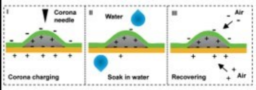	EVA/Silver/BOPP laminated cellular film	▪ Surface potential : -4.67 kV	15 days : -4.67 kV → -3 kV (64.2 %)	9
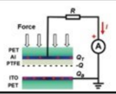	PTFE	▪ Surface potential : -4.62 kV ▪ I_{sc} : 14.7 μA ▪ Transfer charge : 119.2 nC	2 days : -4.62 kV → -1.75 kV (37.9%) 15 days : -4.62 kV → -1.22 kV (26.4 %)	10
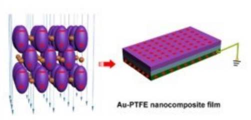	Au NPs-PTFE nanocomposite film	▪ Surface potential : -0.34 kV ▪ V_{oc} : 235 V ▪ I_{sc} : 22 μA ▪ Transfer charge : 135 nC ▪ Surface charge density : 85 μC m^{-2}	20 min : -0.34 kV → -0.26 kV (76.5 %) 30 days : -0.34 kV → -0.21 kV (61.8 %)	11
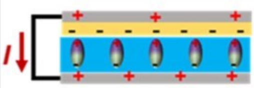	FEP	▪ Surface potential : -1.08 kV ▪ V_{oc} : 105 V ▪ J_{sc} : 137 mA m^{-2} ▪ Surface charge density : 470 μC m^{-2}	6 min : -1.08 kV → -0.73 kV (67.6 %)	12
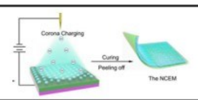	PDMS matrix (PTFE NPs) /PTFE	▪ Surface potential : -2.42 kV ▪ I_{sc} : 150 μA ▪ Transfer charge : 220 nC	25 days : -2.42 kV → -2.34 kV (96.7 %)	13

References

1. J. Comyn, *Int. J. Adhes. Adhes.*, 1992, **12**, 145–149.
2. Y. P. Xie, Z. B. Yu, G. Liu, X. L. Ma and H.-M. Cheng, *Energy Environ. Sci.*, 2014, **7**, 1895–1901.
3. J. W. Lee, H. J. Cho, J. Chun, K. N. Kim, S. Kim, C. W. Ahn, I. W. Kim, J.-Y. Kim, S.-W. Kim, C. Yang and J. M. Baik, *Sci. Adv.*, 2017, **3**, e1602902.
4. K. Xia, Z. Zhu, J. Fu, Y. Li, Y. Chi, H. Zhang, C. Du and Z. Xu, *Nano Energy*, 2019, **60**, 61–71.
5. J. W. Lee, S. Jung, T. W. Lee, J. Jo, H. Y. Chae, K. Choi, J. J. Kim, J. H. Lee, C. Yang and J. M. Baik, *Adv. Energy Mater.*, 2019, **9**, 1901987.
6. J. Peng, H. Zhang, Q. Zheng, C. M. Clemons, R. C. Sabo, S. Gong, Z. Ma and L.-S. Turng, *Nanoscale*, 2017, **9**, 1428–1433.
7. R. Wen, J. Guo, A. Yu, J. Zhai and Z. L. Wang, *Adv. Funct. Mater.*, 2019, **29**, 1807655.
8. J. Qian, J. He, S. Qian, J. Zhang, X. Niu, X. Fan, C. Wang, X. Hou, J. Mu, W. Geng and X. Chou, *Adv. Funct. Mater.*, 2020, **30**, 1907414.
9. J. Zhong, Q. Zhong, G. Chen, B. Hu, S. Zhao, X. Li, N. Wu, W. Li, H. Yu and J. Zhou, *Energy Environ. Sci.*, 2016, **9**, 3085–3091.
10. F. Yuan, W. Li, S. Lin, N. Wu, S. Chen, J. Zhong, Z. Xu, X. Li, Y. Xiao and L. Huang, *Nanoscale*, 2017, **9**, 18529–18534.
11. B. D. Chen, W. Tang, C. Zhang, L. Xu, L. P. Zhu, L. J. Yang, C. He, J. Chen, L. Liu, T. Zhou and Z. L. Wang, *Nano Res.*, 2018, **11**, 3096–3105.
12. Z. Xu, J. Duan, W. Li, N. Wu, Y. Pan, S. Lin, J. Li, F. Yuan, S. Chen, L. Huang, B. Hu and J. Zhou, *ACS Appl. Mater. Interfaces*, 2019, **11**, 3984−3989.
13. H. Li, Z. Guo, S. Kuang, H. Wang, Y. Wang, T. Wu, Z. L. Wang and G. Zhu, *Nano Energy*, 2019, **64**, 103913.